Ultrathin multi-band planar metamaterial absorber based on standing wave resonances

Peng, Xiao-Yu; Wang, Bing; Lai, Shumin; Zhang, Dao Hua; Teng, Jing Hua

2012

Peng, X.-Y., Wang, B., Lai, S., Zhang, D. H., & Teng, J. H. (2012). Ultrathin multi-band planar metamaterial absorber based on standing wave resonances. Optics express, 20(25), 27756-27765.

https://hdl.handle.net/10356/100404

https://doi.org/10.1364/OE.20.027756

Ultrathin multi-band planar metamaterial absorber based on standing wave resonances

Xiao-Yu Peng,[1, 4] Bing Wang,[1] Shumin Lai,[2] Dao Hua Zhang,[3] and Jing-Hua Teng[1,*]

[1]*Institute of Materials Research and Engineering, A*STAR, 3 Research Link, 117602, Singapore*
[2]*National Junior College, 37 Hillcrest Rd, 288913, Singapore*
[3]*School of Electrical and Electronic Engineering, Nanyang Technological University, 639798, Singapore*
[4]*pengxy@imre.a-star.edu.sg*
[*]*jh-teng@imre.a-star.edu.sg*

Abstract: We present a planar waveguide model and a mechanism based on standing wave resonances to interpret the unity absorptions of ultrathin planar metamaterial absorbers. The analytical model predicts that the available absorption peaks of the absorber are corresponding to the fundamental mode and only its odd harmonic modes of the standing wave. The model is in good agreement with numerical simulation and can explain the main features observed in typical ultrathin planar metamaterial absorbers. Based on this model, ultrathin planar metamaterial absorbers with multi-band absorptions at desired frequencies can be easily designed.

OCIS codes: (050.6624) Subwavelength structures; (160.3918) Metamaterials; (260.5740) Resonance.

References and links

1. X. Zhang and Z. Liu, "Superlenses to overcome the diffraction limit," Nat. Mater. **7**(6), 435–441 (2008).
2. C. M. Soukoulis and M. Wegener, "Past achievements and future challenges in the development of three-dimensional photonic metamaterials," Nat. Photonics **5**, 523–530 (2011).
3. N. I. Landy, S. Sajuyigbe, J. J. Mock, D. R. Smith, and W. J. Padilla, "Perfect Metamaterial Absorber," Phys. Rev. Lett. **100**(20), 207402 (2008).
4. X. Liu, T. Starr, A. F. Starr, and W. J. Padilla, "Infrared spatial and frequency selective metamaterial with near-unity absorbance," Phys. Rev. Lett. **104**(20), 207403 (2010).
5. B. Zhang, Y. Zhao, Q. Hao, B. Kiraly, I.-C. Khoo, S. Chen, and T. J. Huang, "Polarization-independent dual-band infrared perfect absorber based on a metal-dielectric-metal elliptical nanodisk array," Opt. Express **19**(16), 15221–15228 (2011).
6. Y. Jin, S. Xiao, N. A. Mortensen, and S. L. He, "Arbitrarily thin metamaterial structure for perfect absorption and giant magnification," Opt. Express **19**(12), 11114–11119 (2011).
7. X. Shen, T. J. Cui, J. Zhao, H. F. Ma, W. X. Jiang, and H. Li, "Palarization-independent wide-angle triple-band metamaterial absorber," Opt. Express **19**(10), 9401–9407 (2011).
8. H. Li, L. H. Yuan, B. Zhou, X. P. Shen, Q. Cheng, and T. J. Cui, "Ultrathin multiband gigahertz metamaterial absorbers," J. Appl. Phys. **110**(1), 014909 (2011).
9. L. Li, Y. Yang, and C. Liang, "A wide-angle polarization-insensitive ultra-thin metamaterial absorber with three resonant modes," J. Appl. Phys. **110**(6), 063702 (2011).
10. P. Ding, E. Liang, G. Cai, W. Hu, C. Fan, and Q. Xue, "Dual-band perfect absorption and field enhancement by interaction between localized and propagating surface plasmons in optical metamaterials," J. Opt. **13**(7), 075005 (2011).
11. Z. H. Jiang, S. Yun, F. Toor, D. H. Werner, and T. S. Mayer, "Conformal dual-band near-perfectly absorbing mid-infrared metamaterial coating," ACS Nano **5**(6), 4641–4647 (2011).
12. Y. Ma, Q. Chen, J. Grant, S. C. Saha, A. Khalid, and D. R. S. Cumming, "A terahertz polarization insensitive dual band metamaterial absorber," Opt. Lett. **36**(6), 945–947 (2011).
13. J. Grant, Y. Ma, S. Saha, A. Khalid, and D. R. S. Cumming, "Polarization insensitive, broadband terahertz metamaterial absorber," Opt. Lett. **36**(17), 3476–3478 (2011).
14. H.-T. Chen, "Interference theory of metamaterial perfect absorbers," Opt. Express **20**(7), 7165–7172 (2012).
15. Q.-Y. Wen, H.-W. Zhang, Y.-S. Xie, Q.-H. Yang, and Y.-L. Liu, "Dual band terahertz metamaterial absorber: Design, fabrication, and characterization," Appl. Phys. Lett. **95**(24), 241111 (2009).
16. H.-T. Chen, J. Zhou, J. F. O'Hara, F. Chen, A. K. Azad, and A. J. Taylor, "Antireflection coating using metamaterials and identification of its mechanism," Phys. Rev. Lett. **105**(7), 073901 (2010).

#174856 - $15.00 USD Received 23 Aug 2012; revised 26 Oct 2012; accepted 14 Nov 2012; published 29 Nov 2012

17. J. Sun, L. Liu, G. Dong, and J. Zhou, "An extremely broad band metamaterial absorber based on destructive interference," Opt. Express **19**(22), 21155–21162 (2011).
18. L. Li, Y. Yang, and C. Liang, "A wide-angle polarization-insensitive ultra-thin metamaterial absorber with three resonant modes," J. Appl. Phys. **110**(6), 063702 (2011).
19. J. Zhou, H.-T. Chen, T. Koschny, A. K. Azad, A. J. Taylor, C. M. Soukoulis, and J. F. O'Hara, "Application of metasurface description for multilayered metamaterils and an alternative theory for metamaterial perfect absorber," arXiv: 1111.0343v1 (2011).
20. Y. Zeng, H.-T. Chen, and D. A. R. Dalvit, "A reinterpretation of the metamaterial perfect absorber," arXiv: 1201.5109 (2012).
21. J. Hao, L. Zhou, and M. Qiu, "Nearly total absorption of light and heat generation by plasmonic metamaterials," Phys. Rev. B **83**(16), 165107 (2011).
22. F. Wooten, *Optical Properties of Solids* (Academic Press, 1972).
23. D. Y. Shchegolkov, A. K. Azad, J. F. O'Hara, and E. I. Simakov, "Perfect subwavelength fishnetlike metamaterial-based film terahertz absorbers," Phys. Rev. B **82**(20), 205117 (2010).
24. M. B. Pu, C. G. Hu, M. Wang, C. Huang, Z. Y. Zhao, C. T. Wang, Q. Feng, and X. G. Luo, "Design principles for infrared wide-angle perfect absorber based on plasmonic structure," Opt. Express **19**(18), 17413–17420 (2011).
25. Y. Q. Ye, Y. Jin, and S. He, "Omnidirectional, polarization-insensitive and broadband thin absorber in the terahertz regime," J. Opt. Soc. Am. B **27**(3), 498–504 (2010).

1. Introduction

Metamaterials have attracted much attention in the past decade for their exotic properties and interesting physics [1, 2]. One important topic is to design so called "perfect absorber" based on fundamental resonance of the oscillators [3–6], which exhibits the ability to yield near-unity absorption by manipulating the effective electrical permittivity, ε, and magnetic permeability, μ. A typical metamaterial based perfect absorber consists of three layers: a metallic structure (unit cells) on the top layer, an opaque metal plane as the ground layer, and a middle dielectric spacer. By adjusting the shape, size, thickness, and properties of metallic structure and dielectric spacer, the absorption frequency and amplitude can be tuned. Due to the nature of sharp resonance response with high quality factor, these absorbers typically exhibit narrow operating bandwidths which only has advantages in some applications such as narrowband filtering, frequency selection, sensing and modulation. For other applications such as solar energy harvesting and high efficiency signal detection, a broadband perfect absorber is desired. Many efforts have been put in to try to enlarge the respond band. So far, dual- or triple-band ultrathin perfect absorbers with single layer metamaterial structure have been realized in microwave [7–9], visible [10], infrared [11], and terahertz wave [12] and some broadband absorbers with multi layer structure [13] had been proposed.

To interpret the phenomena observed from ultrathin planar metamaterial absorbers, several models and theories have been proposed. In the effective medium model [6], the unity absorption was attributed to the effective impedance $Z = (\mu / \varepsilon)^{1/2}$ matching to the free space impedance Z_0 at the resonant frequencies and this impedance matching has been believed to involve and rely on magnetic resonant response with direct evidence from anti-parallel surface currents. However, multiple reflections interference model [14] reveals that the two layers of metal structure in metamaterial absorbers are linked only by multiple reflections with negligible near-field interactions or magnetic resonances. The transmission line model [15] explains the absorber based on LC resonance of the electric split-ring-resonator (eSRR) structure but is limited to only weak couplings between the eSRR and wires layer, and normal incidence of the electromagnetic (EM) wave. Fabry-Pérot resonance model [16, 17] and the multiple reflections interference model [14] can explain well the unity absorptions for those metamaterial absorbers with the thickness d of the spacer to be at least a quarter wavelength λ, i. e. $d = \lambda / (4n)$,where n is the refractive index of the dielectric spacer material. However, Typical Fabry-Pérot resonance model is not good at interpreting the unit absorptions in the case of the ultrathin planar metamaterial absorbers, in which the thickness of the spacer could be much less than the incident EM wavelength i. e. $d << \lambda/4n$. For example, some absorbers have been shown as thin as $\lambda/40$ [8] and $\lambda/69$ [18]. Recently, a modified Fabry-Pérot

#174856 - $15.00 USD Received 23 Aug 2012; revised 26 Oct 2012; accepted 14 Nov 2012; published 29 Nov 2012

resonance model [19] was proposed and provided an alternative interpretation of ultrathin metamaterial-based perfect absorption. Further analysis [20] proved that the appearance of two almost, but not exactly out-of-phase currents inside a metamaterial was necessary for a perfect absorber and although evanescent waves do not contribute to far fields scattered by the perfect absorber, they consume the electromagnetic energy significantly.

In this paper, we analyze the perfect absorption phenomena of the metamaterial absorber from different view. We propose a planar waveguide model and the standing wave resonance mechanism to interpret the absorption phenomena in a typical planar metamaterial absorber. In this model, two metallic layers with the dielectric spacer in between is considered as a planar metal-insulator-metal waveguide and the EM waves from adjacent gaps propagating oppositely in the spacer layer result in standing wave resonances in the waveguide. The standing wave dissipates in the lossy dielectric spacer layer, contributing to the absorption peaks of the metamaterial absorber. The model can well explain the phenomena of waveguide-style ultrathin metamaterial absorbers reported before and can be easily used to design an absorber with the desirable multi-absorption peaks.

2. Theory

The planar waveguide model is schematically exhibited in Fig. 1(a). For the sake of simplicity, we assume that the unit cell of the planar absorber consisting of a rectangle metallic patch on the top layer with the dimensions of $L \times P$, a ground metallic layer, and a dielectric spacer layer with thickness of d in between. The refract index of the spacer layer is *n*, which is a function of frequency f (or wavelength λ) of the incident EM wave. The periodicity in *y* direction is P ($= L + d_c$), where d_c is the gap distance between unit cells and is smaller than λ. The thicknesses of both metallic layers are larger than their skin depth, meaning that no EW wave can penetrate them. The zero position of *x*, *y*, and *z* direction was set at the symmetrical center of the rectangle patch and the interface between the top metallic structure and the spacer layer, respectively. Assuming a plan wave incident normally at the surface of the absorber from air, with electric field $\boldsymbol{E}_0$, magnetic field $\boldsymbol{H}_0$, and wave vector $\boldsymbol{k_0}$ ($k_0 = 2\pi / \lambda_0$). When the incident EM wave impinges the gaps, it is diffracted into the spacer layer then reflected by the ground metallic layer, then guided into the dielectric spacer layer between two metallic layers. The diffracted EM wave has electric field $\boldsymbol{E}$, magnetic field $\boldsymbol{H}$, and wave vector $\boldsymbol{k}$ ($k = nk_0 = 2\pi n / \lambda_0$). Considering the case of electric field in the incident plane (TM polarized) as shown in Fig. 1(a), the diffracted wave can be separated into two components: the wave propagating along the *y* direction with electric field $E_y = E \sin\theta$ and wave vector $k_y = k \sin\theta$ and the wave propagating along the *z* direction with electric field $E_z = E \cos\theta$ and wave vector $k_z = k \cos\theta$. The relations among three vectors and their components are zoomed and shown in Fig. 1(b). Due to the symmetrical design, the guided EM waves from adjacent gaps propagate oppositely and combine to form a standing wave in the waveguide. The waves propagating along the + *y* direction and –*y* direction can be represented by the equations below:

$$E_z^+ = E_{z0} \exp[i\,(k_y y - \omega_0 t + \phi_0 + \pi)] \tag{1}$$

And

$$E_z^- = E_{z0} \exp[i\,(-k_y y - \omega_0 t + \phi_0)] \tag{2}$$

Here $\varnothing_0$ is the initial phase of the incident EM wave. Due to the thickness of spacer $d \ll L$, we only consider the attenuation in the *y* direction. Thus the amplitude of the guided EM wave $E_{z0} = E \exp\left[-\mu\left(\frac{L}{2}\right) - |y|\right]\sin\theta$, where μ is the attenuation coefficient of the lossy

#174856 - $15.00 USD Received 23 Aug 2012; revised 26 Oct 2012; accepted 14 Nov 2012; published 29 Nov 2012

dielectric material of the spacer layer, $\boldsymbol{\theta}$ is the diffraction angle, and the angular frequency of the incident EM wave $\omega_0 = 2\pi f_0 = 2\pi c / \lambda_0$, c is the velocity of EM wave in vacuum. The superposition of two opposing waves forms a standing wave and its equation can be expressed as:

$$E_{zsw} = E_z^+ + E_z^- = -2E \sin\theta \exp\left[-\mu\left(\frac{L}{2} - |y|\right)\right] \sin\left(\frac{2\pi n \sin\theta}{\lambda_0}\right) \sin\left(\frac{2\pi c}{\lambda_0} t + \phi_0\right) \quad (3)$$

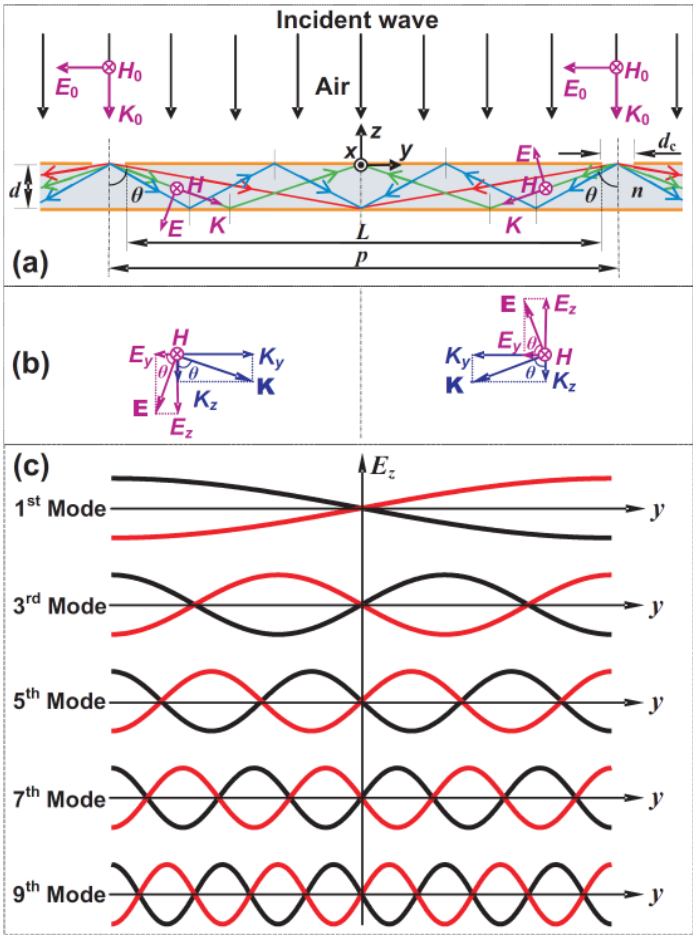

Fig. 1. Illustration of standing wave resonance model of a typical ultrathin planar metamaterial absorber. (a) Structure of the waveguide and the incident EM wave; (b) Zoomed vectors and their components of the diffractive EM waves from adjacent gaps; (c) Normalized electric field of the fundamental mode and its odd harmonic modes at x = 0 and z = - d/2 in the case of strong diffraction effect calculated according to Eq. (3).

At locations $y = \pm j \dfrac{\lambda_0}{2n \sin\theta}$, j = 0, 1, 2, 3…, the amplitude is always zero, are the nodes. Whereas the anti-nodes are located at $y = \pm(2j-1)\dfrac{\lambda_0}{4n \sin\theta}$, j = 1, 2, 3…, are the locations of maximum loss energy densities. Considering the symmetrical geometry and the free boundary conditions at both ends of a unit cell, the symmetrical centre is always a node and both ends

#174856 - $15.00 USD Received 23 Aug 2012; revised 26 Oct 2012; accepted 14 Nov 2012; published 29 Nov 2012

of the unit cell are the anti-nodes. Therefore only following resonant modes of the standing wave are possible:

$$f_{sw} = (2j-1)\frac{c}{2nL\sin\theta}, j = 1,2,3,... \quad (4)$$

Or

$$\lambda_{sw} = \frac{2nL\sin\theta}{(2j-1)}, j = 1,2,3,... \quad (5)$$

where L is the length of the top layer rectangular patch and it can be thought as the rough length of the planar waveguide. Considering the ultrathin condition ($\lambda_0 >> d$), the higher order metal-insulator-metal waveguide modes are evanescent and only the fundamental waveguide mode is allowed to propagate along the waveguide, therefore we have $\sin\theta \approx 1$, Eqs. (4) and (5) may be simplified as:

$$f_{sw} \approx (2j-1)\frac{c}{2nL}, j = 1,2,3,... \quad (6)$$

Or

$$\lambda_{sw} \approx \frac{2nL}{(2j-1)}, j = 1,2,3,... \quad (7)$$

Equations (4) to (7) indicate that only the fundamental standing wave mode (j = 1) and its odd harmonic modes are available, as can be seen in Fig. 1(c). The results agree with ref [21]. that the second-order mode could not be excited for normally incident light. These modes correspond to the absorption peaks of the metamaterial absorber. Given a target frequency f_1 (the 1st mode or fundamental mode, corresponding to j = 1) of the absorption peak and the refractive index $n(f_1)$ or $n(\lambda_1)$ of the dielectric spacer material at this frequency f_1 (or wavelength λ_1), the dimension L of the top layer planar metamaterial structure of the absorber may be easily estimated according to following equation:

$$L \approx \frac{\lambda_1}{2n(\lambda_1)} = \frac{c}{2n(f_1)f_1} \quad (8)$$

Above discussion is based on the TM polarization of incident EM wave. In contrast, for the TE polarization of incident EM wave, i.e. the electric component E of EM wave is perpendicular with yz plane, no standing wave resonance of the electric field can be formed in the waveguide. Hence, no corresponding absorption peaks can be observed.

3. Simulation results and discussion

To validate our model, we performed simulations using CST Microwave Studio. The typical absorber is designed working at terahertz (THz) range in which the plasmonic effect is weak, consisting of a periodic array of alumina (Al) rectangle patch, an Al ground plane and a thin lossy silicon dielectric layer in between. One of the unit cells from the front view is shown at the top in Fig. 2(a), with the rectangle dimension L = 60 μm in y direction and the periodicity $P = L + d_c = 70\mu m$, The zoomed cross section of a unit cell with three layer structures is shown at the bottom with Si spacer layer thickness of d = 3.4 μm. The thicknesses of both metallic layers are set as 0.2 μm to guarantee no transmission of EW wave through them. The substrate is used to support the whole structure. A plane wave was incident from top onto the Al square. The conductivity of Al was assumed as 3.72×10^7 S/m in our numerical simulations. Since every absorption peak has its own thickness d of the

#174856 - $15.00 USD Received 23 Aug 2012; revised 26 Oct 2012; accepted 14 Nov 2012; published 29 Nov 2012

spacer, we optimize the thickness d of the lossy silicon layer at 3.4 μm with most number of perfect absorption peaks.

The absorption spectra of TM polarized THz waves are shown in Fig. 2(b) in black. One can observe that there are eight distinct narrow absorption peaks distributing across the entire THz band at frequencies of f_1 = 0.667 THz, f_2 = 2.02 THz, f_3 = 3.35 THz, f_4 = 4.63 THz, f_5 = 5.65 THz, f_6 = 6.49 THz, f_7 = 7.49 THz, and f_8 = 7.87 THz, respectively. Among these peaks,

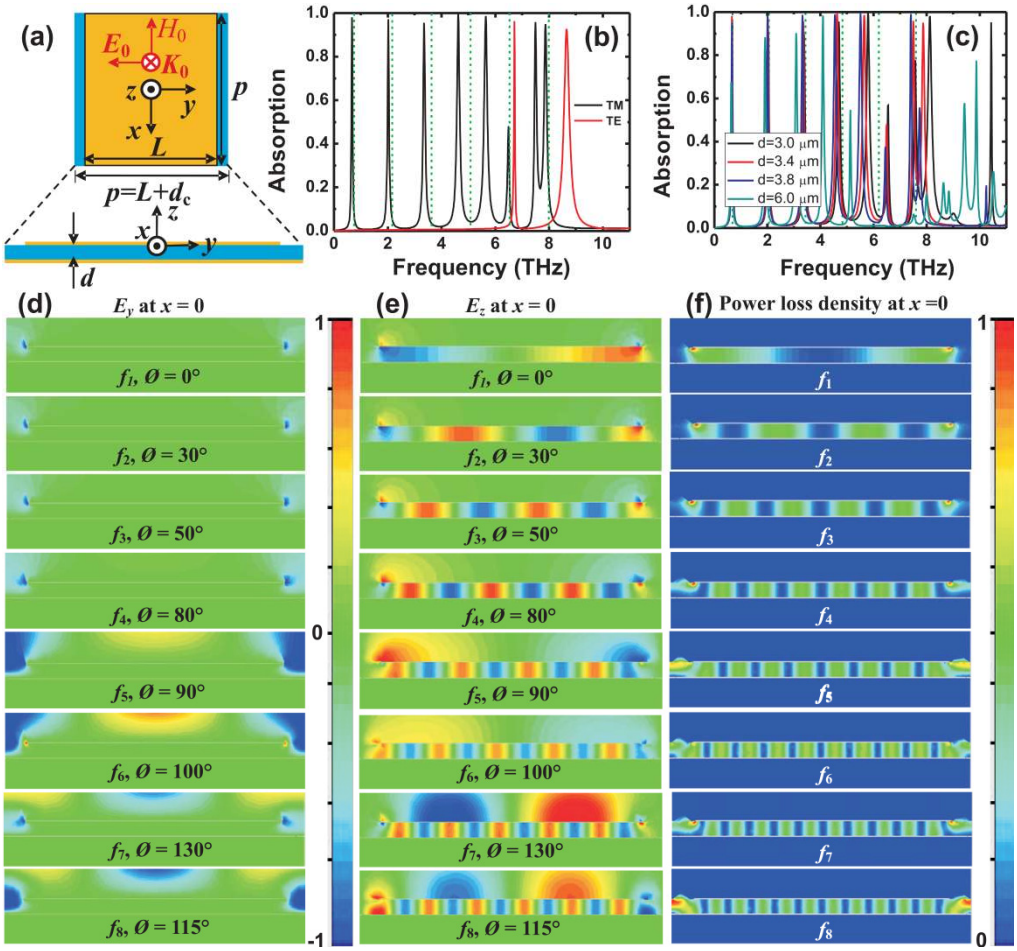

Fig. 2. Diagram of the ultrathin THz planar metamaterial absorber based on standing wave resonances and the simulation results in the case of incident wave with TM polarization. (a) Front view at the top and side view at the bottom of the structure; (b) Simulated absorption spectra induced by incident EM wave with TM (black line) and TE Polarization (red line). The dashed line represents the frequencies of the standing wave modes calculated according to Eq. (6). (c) Simulated absorption vs. the thickness d of the dielectric spacer layer of the absorber; (d) Electric field component E_y at $x = 0$ corresponding to different absorption peaks at different phase when the strength of E_y is strongest; (e) Electric field component E_z at $x = 0$ corresponding to different absorption peaks at different phase when the strength of E_z is strongest; (f) The power loss density distribution at $x = 0$.

seven have absorption strengths greater than 90% and some peaks achieve nearly perfect absorption- with strengths>99%. Seven peaks correspond to the frequencies as seen in Fig. 2(b), the frequency intervals between two adjacent peaks are nearly same from f_1 to f_4, indicating that f_2 to f_4 are the odd harmonics of f_1. We compared the frequency positions of the peaks from simulation results with that of the fundamental mode and its odd harmonic modes calculated with Eq. (6), showed by dashed green vertical lines in Fig. 2(b). In the

#174856 - $15.00 USD Received 23 Aug 2012; revised 26 Oct 2012; accepted 14 Nov 2012; published 29 Nov 2012

calculation the refract index of silicon layer is set as 3.4496 within entire THz range by using the equation $n = \left\{ \left[\left(\varepsilon_r^2 + \varepsilon_i^2 \right)^{1/2} + \varepsilon_r \right] / 2 \right\}^{1/2}$ [22]. One can see calculated results from Eq. (6) matched very well with the simulation results for the fundamental mode (f_1). The small discrepancy is due to that the real length of the waveguide is larger than the top Al rectangle patch. The discrepancy becomes larger with increasing mode order. This is because the higher the order of the mode, the more sensitivity to the change of thickness of the spacer layer. In the case of higher frequency range, f_5 to f_8 do not comply with the same rule, indicating that the main absorption mechanism is different from the lower frequency range from f_1 to f_4 if the wavelength of incident EM wave is comparable with the gap dimension. There are no fundamental and its harmonics observed in the case of TE polarization of incident THz wave as shown in Fig. 2(b) in red.

We change the thickness d of dielectric layer to investigate how it affects the absorption peaks. As can be seen in Fig. 2(c), not only the amplitude of each peak is changed but the peaks are red shifted with the increase of d. The absorption peaks at higher frequency are more sensitive to the change of d. With the same increment of d, the higher frequency of the absorption peak, the larger the red shift of the absorption peak will be. When the change of d is small, such as changing from 3 to 4 μm, the red shifts of f_1 and f_2 peaks are too small to be clearly observed. It should be mentioned that, for f_1 this small change of d does not affect the fact that $d < \lambda/100$, the reason why the absorber is called "untrathin".

To further understand the absorption mechanisms, we simulated the electric field distribution of the absorber structure in the case of TM polarization of incident THz wave. Since the x component of electric field E_x is zero through entire the structure apart from only a very small distribution limited at the edges of the rectangle patches, we only present the distributions of E_y and E_z at $x = 0$ corresponding to different absorption peaks with frequencies from f_1 to f_8 at different phase Φ_0 that corresponding to the strongest electric field for each frequency, as shown in Figs. 2(d) and 2(e), respectively. For the simplicity, we use the normalized scale to present each E_y and E_z. As can be seen, from f_1 to f_4, E_y is small and only limited around the edges of the rectangle patch while E_z shows the typical fundamental standing wave mode and its 3rd, 5th, and 7th harmonic modes, respectively. Clearly, the standing wave resonance is the main mechanism for the absorption peaks corresponding to f_1 to f_4. From f_5, E_y becomes stronger and distributes nearly the whole gaps. This is because the diffraction effect becomes weaker with the increase of frequency of the incident THz wave. Note that near the ground plane the E_y is always zero due to the superposition of the incident wave and the reflected wave with anti-phase. From f_5 to f_8, the E_z shows the 7th, 9th, 11th and 11th harmonics of the standing wave, respectively. Comparing the strength of E_y and E_z of same frequency, we find that E_y become stronger and E_z becomes weaker with the increase of frequency. In the case of f_8, $E_y > E_z$, indicates that the mechanism of the superposition of E_y in the gaps play a more important role for the absorption of incident EM wave.

Above analysis can be further identified with the power loss density distribution. Since the surface power loss density (Ohmic loss on the metallic layers) is around 5 orders of magnitude smaller than that of in the spacer layer, here we only present the power loss density in the dielectric layer at $x = 0$ as shown in Fig. 2(f). One can see clearly that the patterns of the power loss density in the dielectric layer corresponding to each absorption peak are similar to the standing wave modes shown in Fig. 2(e), denotes that most energy of the incident EM wave is dissipated in the dielectric layer between two metallic layers through the standing wave resonance mechanism. On the other hand, the incident THz wave with TE polarization does not induce the standing wave modes of electric field. The main mechanism for the two absorption peaks within 6-10 THz for the incident THz wave with TE polarization as shown in Fig. 2(b) is the resonance of the superposition of incident THz wave and its reflected wave in the gaps.

#174856 - $15.00 USD Received 23 Aug 2012; revised 26 Oct 2012; accepted 14 Nov 2012; published 29 Nov 2012

It should be noted that Fig. 2(c) only show the pattern of standing wave modes at $x = 0$. Actually the electric field of the standing waves distributes in the whole area under the rectangle Al patch. An example of 2D electric field patterns at the central plane of spacer layer (z = - 1.7μm) corresponding to eight absorption peaks are shown in Fig. 3. Apparently the shapes of patterns are relevant to the shape of the top metallic plane.

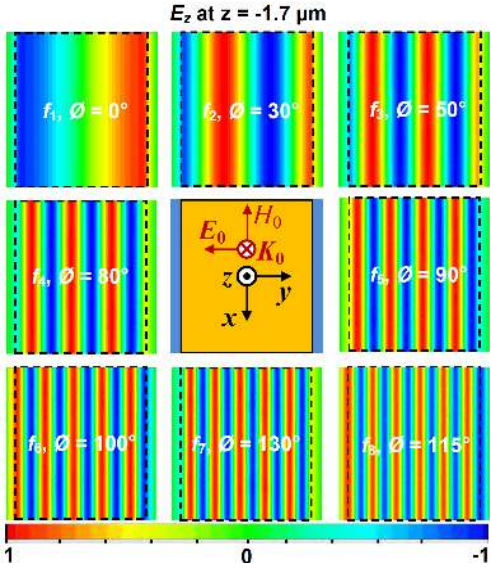

Fig. 3. Distributions of electric field component Ez at z = −1.7μm corresponding to eight absorption peaks shown in Fig. 2(b) in the case of incident EM wave with TM polarization. The inset shows the front view of the unit cell.

We also validated our model by using it to explain the phenomena observed in other reported absorbers in which their structures could be treated as planar waveguides. For example, the infrared near-unity absorber with cross-shaped resonator [4], frequency-selective surface (FSS) of a fishnet structure with rectangular or cross openings [23], the infrared wide-angle absorber with circular plates [24], and the planar absorber with no second-order harmonic mode excited for normally incident light [21] *et. al*. can all be explained and demonstrated with our model. These published papers have demonstrated their perfect planar metamaterial absorbers with so called ultrathin single-band (one absorption peak), which actually corresponded to the fundamental modes of the standing waves in the waveguide structures since only a small frequency or wavelength range was investigated. As an example, here we present our simulation results that come from an infrared planar absorber with a cross-shaped resonator in one unit cell, in which all the parameters are similar to ref [4]. The structure is shown in Fig. 4(a), in which L = 1.7 μm, p = 2.0 μm, w = 0.4 μm, d = 0.13 μm. The golden cross and the golden ground plane constitute a waveguide. The dielectric constant ε_r and loss tangent ε_i of the Al_2O_3 dielectric spacer are 2.28 and 0.04, respectively. The absorption spectrum is shown in Fig. 4(b). Here we focus on the absorption peak due to the contribution of the fundamental standing wave resonance formed in the dielectric layer between the transverse strip (marked as "I") of the metallic cross and the ground plane as shown in the inset of Fig. 4(a). To compare the simulation results with our model, we calculate the frequency corresponding to the fundamental mode f_1. f_1 is calculated according to Eq. (7) of our model. It is 58.43 THz as shown in Fig. 4(b) with dashed green line. As can be seen in Fig. 4(b), the calculation result 58.43 THz with our model is in good agreement with the simulation result that the frequency of the peak position is 57.5 THz. The electric component E_z at $x = 0$ shown in Fig. 4(c) and E_z at z = - 0.065 μm (the central plane

#174856 - $15.00 USD Received 23 Aug 2012; revised 26 Oct 2012; accepted 14 Nov 2012; published 29 Nov 2012

of the spacer) in Fig. 4(d) also indicate the fundamental standing wave mode formed in the spacer layer between the strip I and the ground plane.

As to the multilayer planar metamaterial absorbers with different dimensional cross-shaped resonators [13, 25], they can also be treated as multi layer planar waveguides with different length hence the multi-band or broadband absorption can be interpreted with our model. It should be noted that our model is suitable for the demonstration of the ultrathin planar metamaterial absorbers with two metallic layers that can be treated as a planar waveguide and in the case of strong diffraction of the incident EM wave.

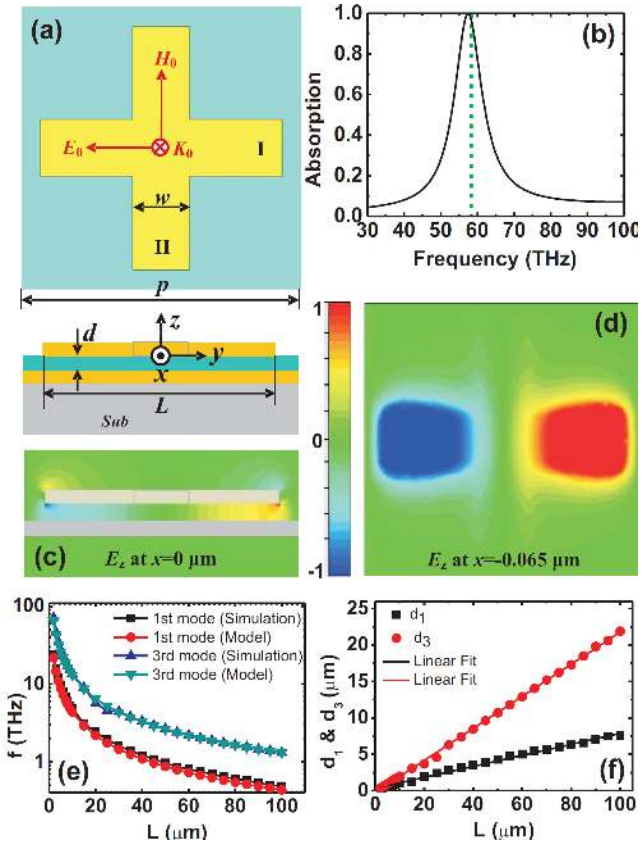

Fig. 4. Ultrathin planar metamaterial absorber with a cross metallic top layer. (a) The front view of the unit cell (top) and the side view of the unit cell (bottom); (b) Simulation result of the absorption spectrum of an infrared absorber. The dashed line represents the fundamental mode calculated with Eq. (6). (c) Electric field component E_z at x = 0 μm; (d) Electric field component E_z at z = - 0.065 μm. (e) Simulation results of the 1st and 3rd modes of the cross-waveguide style absorber working at the infrared and THz domain vs. the results calculated with Eq. (6) at different dimension L of the cross. (f) Simulation results of the optimized thicknesses d_1 and d_3 corresponding to the 1st and the 3rd modes at different dimension of the cross, respectively. The straight lines are the linear fits.

Based on Eqs. (6) to (8) one may easily obtain an ultrathin metamaterial absorber with the expected working frequency. Figure 4(e) shows the frequencies of the 1st and 3rd standing wave mode corresponding to the absorption peaks calculated with our model versus the simulation results at different dimension L of the golden cross layer (shown in Fig. 4(a)) of the planar metamaerial absorbers working at infrared and THz domain. In the simulation, the thickness of both the golden ground and cross layer is 0.2 μm. The periodic parameter P = 1.2L, the width of the strips of the cross is W = 0.1L. The spacer material is silicon with dielectric constant $\varepsilon = 11.9 + 0.004i$. Due to the small change of the refractive index n of

#174856 - $15.00 USD Received 23 Aug 2012; revised 26 Oct 2012; accepted 14 Nov 2012; published 29 Nov 2012

silicon in infrared and THz domain, n is set as a constant 3.4496 in the calculation with our model. It can be seen clearly from Fig. 4(e) that both the calculation results of the 1st and 3rd modes with our model are good in agreement with the simulation results. This agreement further validates our model and indicates that the waveguide-style ultrathin planar metamaterial absorber with an expected working frequency can be easily designed. The optimized thicknesses d_1 and d_3 corresponding to the 1st and 3rd modes (perfect absorption peaks) are obtained from the simulation as shown in Fig. 4(f), respectively. Clearly both d_1 and d_3 increase linearly with the dimension L of the cross and d_3 is larger than d_1 at the same L.

4. Conclusion

In conclusion, we have proposed a planar waveguide model and a simple analytical formula to explain the unity absorption in ultrathin waveguide-style planar metamaterial absorbers based on standing wave resonances. It shows that only the absorption peaks corresponding to the fundamental mode and its odd harmonic modes can be excited. Numerical simulation results verified our model and indicate that the majority of energy is dissipated in the dielectric spacer layer through the standing wave resonances. Our model explains well the main features observed in previously reported planar waveguide-style metamaterial absorbers. It provides a simple way to design multi-band ultrathin planar metamaterial absorbers with expected working frequencies and makes it much easier to design even super broadband ultrathin metamaterial absorbers for potential applications in filters, detectors and energy conversion devices.

Acknowledgments

The first author would like to thank Dr. Ravi S. Hegde and Dr. Yun Tao for their thoughtful discussion related to this work. This work is supported by the A*STAR Metamaterials program under Grant Nos. of 0921540097 and 0921540099 and by the program NRF-G-CRP 2007-01.

#174856 - $15.00 USD Received 23 Aug 2012; revised 26 Oct 2012; accepted 14 Nov 2012; published 29 Nov 2012